Received: 14 April 2020 | Revised: 31 August 2020 | Accepted: 2 November 2020

DOI: 10.1002/sia.6919

RESEARCH ARTICLE

SURFACE and INTERFACE ANALYSIS WILEY

Corrosion protection of the AA2198-T8 alloy by environmentally friendly organic-inorganic sol-gel coating based on bis-1,2-(triethoxysilyl) ethane

Rafael Emil Klumpp[1] | Uyime Donatus[1] | Rejane Maria Pereira da Silva[1] | Renato Altobelli Antunes[2] | Caruline de Souza Carvalho Machado[1] | Mariana Xavier Milagre[1] | João V. de Sousa Araujo[1] | Bárbara Victoria Gonçalves de Viveiros[1] | Isolda Costa[1]

[1]Instituto de Pesquisas Energéticas e Nucleares, São Paulo, São Paulo, Brazil

[2]Centro de Engenharia, Modelagem e Ciências Sociais Aplicadas (CECS), Universidade Federal do ABC (UFABC), Santo André, São Paulo, Brazil

Correspondence
Rafael Emil Klumpp, Instituto de Pesquisas Energéticas e Nucleares, Av. Prof. Lineu Prestes, 2242, São Paulo, São Paulo, Brazil.
Email: rafahemil@hotmail.com

Funding information
Conselho Nacional de Desenvolvimento Científico e Tecnológico (CNPq), Grant/Award Number: 426280/2016-4

In this work, a surface coating composed of organic-inorganic hybrid sol-gel based on bis-1,2-(triethoxysilyl) (BTSE) ethane was applied on AA2198-T8 samples, and its effect on corrosion resistance was investigated and compared with that of a chromate layer formed in a solution with hexavalent chromium ions. The corrosion resistance of BTSE coated samples was evaluated by immersion tests in sodium chloride solution (0.005 mol/L NaCl) and monitored by global electrochemical techniques such as electrochemical impedance spectroscopy (EIS) and local electrochemical techniques such as scanning vibrating electrode technique (SVET) and scanning electrochemical microscopy (SECM). The formed coating layers were characterized by X-ray photoelectron spectroscopy (XPS). The results pointed out that the BTSE is an effective alternative coating for corrosion protection of new generation Al-Cu-Li alloys and could replace chromates obtained in toxic and carcinogenic CrVI containing solutions leading to improved corrosion protection.

KEYWORDS
AA2198-T8, BTSE, coatings, corrosion, silane

1 | INTRODUCTION

The promising future of new generation Al-Cu-Li alloys is associated with weight reduction and specific strength, amongst other factors.[1,2] Compared with conventional Al-Cu-Mg and Al-Zn-Mg alloys, the new generation of Al-Cu-Li alloys has been developed to exhibit higher specific strength and fracture toughness than conventional alloys and to replace them. However, the development of localized corrosion in the new generation alloys is still a great concern. Severe localized corrosion in Al-Cu-Li alloys has been associated with hexagonal T1 phase (Al_2CuLi), which is preferentially located in regions of high dislocation density.[3–14] This leads to severe localized corrosion.[13,15,16] According to literature,[17,18] T1 phase is initially anodic relatively to the matrix, but due to the high reactivity of lithium, its selective dissolution from T1 phase leads to its copper enrichment, polarity reversal, and, in turn, the dissolution of the surrounding matrix.[16] Severe localized corrosion compromises the structural integrity of alloys and can lead to an early undesirable failure.[17,18]

Surface treatments based on hexavalent chromium have been used for decades, and these are highly effective for corrosion protection of aluminum alloys, in addition to promoting good adherence to organic coatings and self-healing properties.[19–23] However, it is well known that hexavalent chromium is extremely harmful to health (carcinogenic) and to the environment (toxic), and one of the major problems associated with such treatments is the disposal of the waste generated. Currently, the search for surface treatments that are environmentally friendly is highly encouraged.[20] Silane films have been considered potential replacements for chromate coatings in the

protection of aluminum alloys, especially as they are environmentally friendly.[24] The BTSE is described by the formula: R'-Si(R3), where the R' is an organofunctional group that is responsible for the hydrocarbon bond, and R3 is the hydrolysable alkoxy group that reacts with water to produce silanol groups (Si-OH). The R3 groups are condensed into steric groups in solution and are attracted to the oxide on the metal surface by hydrogen bonding during the coating process. Following this, a Si-O-C network is formed on the substrate via a curing/cross-linking process.[25–30]

Many authors have reported success on the use of silane as a pretreatment agent to increase the corrosion resistance of aluminum alloys.[23,26,29,31–33] However, little information about the effect of this kind of treatment on the corrosion resistance of new generation Al-Cu-Li alloys exist in the literature.[1,24,33] The silane chosen for this study is the BTSE [$(H_5C_2O)_3$-Si-CH_2CH_2-Si-$(OC_2H_5)_3$] that has a bis-functional structure with six silanol groups that can provide stronger covalent bonds with metal oxide compared with the one with a mono-functional structure.[34–36] The aim of this study is to investigate the effect of a bis-silane–based treatment for the corrosion protection of the polished and unpolished surfaces of an AA2198-T8 Al-Cu-Li alloy. Comparing the polished and unpolished surfaces of the alloy is very important because the presence of near-surface deformed layers (NSDL), induced by the rolling process employed during the production of rolled Al alloys, affects the corrosion and electrochemical responses of the alloys.[37–41] Furthermore, the effect of the BTSE has also been compared with that of a chromate conversion coating in order to further understand the suitability of BTSE as a replacement for hexavalent chromium-containing treatments.

2 | EXPERIMENTAL

The AA2198-T8 alloy whose chemical composition is presented in Table 1 was used in this study.

Selected samples were polished with diamond paste up to a 1-μm surface finish. Unpolished samples were degreased with ethanol and dried under air stream before use. The polished samples were degreased in ethanol, deoxidized in 1% nitric acid at room temperature for 30 s before a final rinse in deionized water. The BTSE treatment was carried out by immersion for 3 min in a solution with 5% of bis-1,2-(triethoxysilyl) ethane and then oven-dried at 100°C for 30 min. Polished and unpolished samples were also coated with a commercial chromate layer (Alodine 1000), herein, designated CrVI, for comparison. Immersion test in 0.005 mol L^{-1} NaCl solution for up to 12 h with polished and unpolished samples, treated with BTSE or CrVI, was carried out to evaluate and compare the effect of NSDL on the corrosion behavior of the AA2198-T8 alloy. Electrochemical impedance spectroscopy (EIS) tests were performed in triplicate to evaluate the corrosion resistance of the samples after conversion treatments. The tests were accomplished at room temperature in a conventional three-electrode cell, with an Ag/AgCl (KCl saturated) as reference electrode, a platinum wire as counter electrode and the treated samples as working electrode. A solution composed of 0.1 mol L^{-1} NaCl was used as

TABLE 1 Chemical composition (wt%) of the AA2198-T8 used in this study analyzed by ICP-AES

Cu	Li	Mg	Ag	Zr	Fe	Si	Zn	Mn	Al
3.32 ± 0.03	0.96 ± 0.01	0.31 ± 0.00	0.26 ± 0.00	0.51 ± 0.01	0.00498 ± 0.00002	0.00424 ± 0.00006	0.00439 ± 0.00007	0.00180 ± 0.00002	Bal.

electrolyte. EIS measurements were performed in the frequency range from 10^4 to 10^{-2} Hz, with a perturbation amplitude of 10 mV and an acquisition rate of 10 points per decade. For the EIS tests, a Solartron potentiostat model SI 1287, coupled to a frequency response analyzer, Solartron SI 1260, was used.

Scanning vibrating electrode technique (SVET) tests were performed using an Applicable Electronics™ SVET machine controlled by an Automated Scanning Electrode Technique (ASET 4.0) software. An insulated Pt-Ir probe was used as the vibrating electrode for the SVET system. A 15-μm-diameter platinum sphere was electrodeposited at the tip of the probes prior to the start of SVET tests. The amplitude of vibration was 19 μm, and the vibrating frequencies of the probe were 174 Hz (X) and 73 Hz (Z); 35 × 25 points were obtained for each SVET map. The time lag between each current density data-point acquired was 0.5 s, and the scan step interval was 200 μm. All experiments were performed in a Faraday cage at (20 ± 2)°C. The AA2198-T8 alloy sample used as the working electrode was embedded in epoxy resin. Experiments were performed in 0.005 mol L^{-1} NaCl for 24 h, and SVET maps were obtained every 2 h. In situ images of the corroding AA2198-T8 surface were obtained at timed intervals during the SVET measurements.

In order to understand and compare the effect of NSDL on the corrosion behavior of the AA2198-T8 alloy, polished and unpolished samples, treated with BTSE and CrVI, were examined after immersion test in 0.005 mol L^{-1} NaCl solution for 12 h.

Scanning electrochemical microscopy (SECM) was performed using a microscope Sensolytics (GmbH Bochum, Germany). The experiments were performed at room temperature and open circuit potential using a three electrode-cell experimental setup, with 25 μm Pt disk ultramicroelectrode (UME) as working electrode, Ag/AgCl KCl (sat) as reference electrode and a platinum wire as counter electrode. The electrolyte used in the SECM tests was 0.01 mol L^{-1} NaCl solution.

Measurements were carried out at selected heights of the UME above the surface. The operating height was set after recording z-approach curves, with the UME adjusted to 30 μm above the sample. SECM maps in constant height mode was obtained by scanning the UME in the x-y plane. The experiments were performed using the surface generation/tip collection (SG-TC) mode. In this mode, H_2 generation from corrosion at the surface is sensed in an oxidation reaction in the UME (reaction 1):

$$H_2 \rightarrow 2H^+ + 2e^-. \quad (1)$$

The H_2 generated on the surface can be sensed in an oxidation reaction 1 at the Pt UME potential of 0.0 V versus Ag/AgCl.

X-ray photoelectron spectroscopy analysis (XPS) was carried out using a ThermoFisher Scientific K-alpha+ spectrometer operating with a monochromated Al-kα radiation source (1486.6 eV) and a spot size of 400 μm to obtain the maximum signal over the largest area possible. High-resolution spectra were obtained using pass energy of 50 eV. Peak fitting was performed using a mixture of Gaussian-Lorentzian functions in the Avantage™ software with background subtraction by the Smart algorithm. Binding energy scale was calibrated by referencing the C1s value at 284.8 eV.

3 | RESULTS AND DISCUSSION

3.1 | Immersion test and SVET

Optical images of the unpolished BTSE treated surface and CrVI treated surface are shown in Figure 1. No significant corrosion on both surfaces was noticed after 2 h of test. However, after 12 h of immersion, propagation of corrosion attack (dark patches) were seen on both surfaces. These attacks correspond to the electrochemical activities in the dark bands seen in the as-received sample, as shown in Figure 2. These bands have been reported to be enriched in Mg and, consequently, are more active compared with the adjacent regions.[37,42,43] However, the attacks associated with these bands on the NSDL are superficial and rarely result in severe localized corrosion, except if there is an external galvanic influence requiring the sustenance of pronounced cathodic activities on a connected nobler surface.[37]

Presented in Figure 3 are the optical images of the polished BTSE treated surface, Figure 3A,B and CrVI treated surface, Figure 3C,D. Figure 3A,C shows optical images of the polished AA2198 T8 alloy coated with BTSE film and with chromate (CrVI) coating, respectively, after 2 h of exposure to the test solution. After this time, no apparent corrosion feature was observed for both treatments. Interestingly, after 12 h of exposure, the polished and BTSE treated sample presented no corrosion, Figure 3B, whereas a pitting site was observed on the polished AA2198-T8 alloy treated with CrVI containing solution, Figure 3D. It is important to note that the NSDL induced by the manufacturing process was removed by the polishing process. Thus, the polished surfaces are free of enriched Mg bands and are somewhat homogeneous in this regard. The absence of the NSDL enhanced the formation of more uniform and protective BTSE layer on the alloy. For the sample with chromate (CrVI) coating, although the absence of NSDL improved the resistance to generalized corrosion, a site with severe localized corrosion was seen. These results are evident on the SVET maps of the unpolished AA2198-T8 alloy with BTSE coating, Figure 4. The SVET maps showed lower activity for 2 h of exposure compared with 12 h in NaCl. Between 2 and 12 h, the SVET maps showed pronounced increase in the current values, and anodic and cathodic areas were well separated. Figure 5 shows SVET maps of the unpolished AA2198-T8 alloy with chromate (CrVI) coating, and the results were similar to those for the unpolished BTSE coated surface, although slightly higher currents were obtained for samples with BTSE coating compared to chromated ones. However, this last treatment was not enough to eliminate the anodic sites initiated in the Mg-rich bands.

In agreement with the optical images, SVET maps showed that when the alloy surface is polished prior to treatments, the current decreases with time of test, Figures 6 and 7. For the polished surface with BTSE coating, the electrochemical activity was inferior to the of

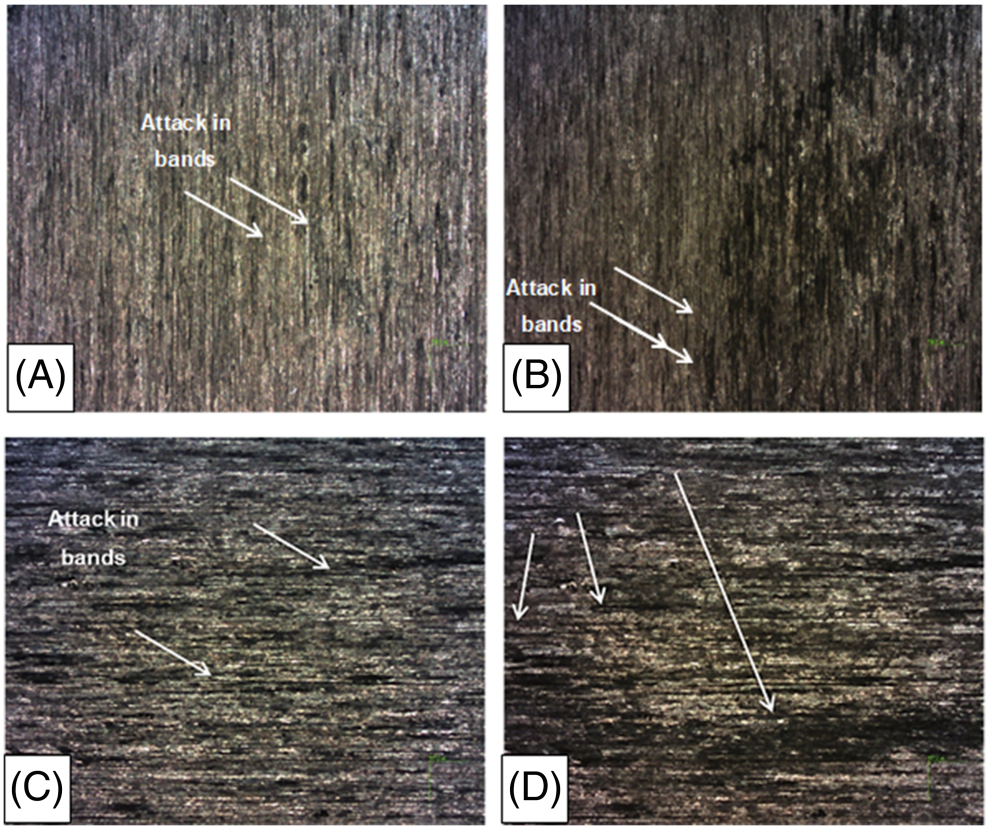

FIGURE 1 Unpolished AA2198 T8 after exposure to 0.005 mol L^{-1} NaCl solution: coated with BTSE silane film for (A) 2 h and (B) 12 h and with chromate coating after (C) 2 h and (D) 12 h

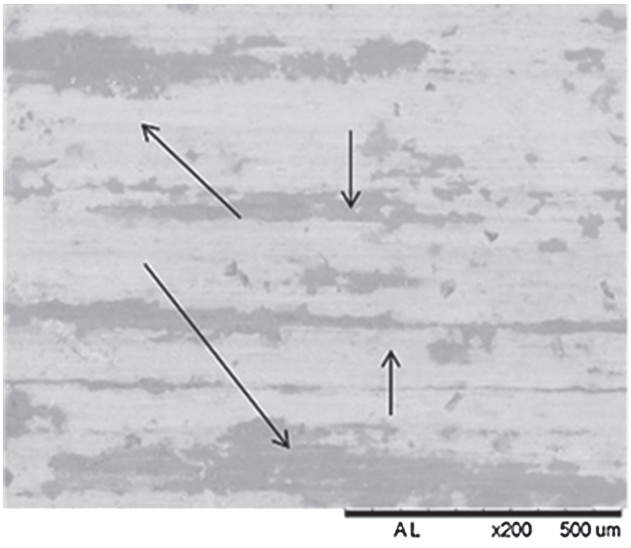

FIGURE 2 Surface of the AA2198 T8 as-received

the AA2198 T8 alloy with chromate (CrVI) coating (Figure 7). In the early hours (Figure 7A), the chromated alloy exhibited very low activities but after 12 h, a pit had developed on the surface; the current densities related to this pit were monitored by SVET, Figure 7B.

3.2 | Electrochemical impedance spectroscopy

EIS results comparing the effects of both coatings, chromate (CrVI) and BTSE, on the corrosion resistance of the polished and unpolished AA2198-T8 after 24 h of exposure to 0.1 mol L^{-1} NaCl solution are shown in Figure 8. Higher impedances were related to the BTSE coated AA2198-T8, Figure 8A, than to the chromated one, Figure 8B showing that the BTSE coating provided improved corrosion protection compared to the chromate coating. The results for the polished AA2198-T8 also showed higher impedances related to the BTSE coated AA2198-T8 than to the chromated one, although the impedance difference between the treatments are lower than for the unpolished samples. These results clearly show that the NSDL affected the corrosion mechanism and the corrosion resistance of the alloy, Figure 9.

EIS results are in agreement with the optical images and SVET results presented earlier. The NSDL showed in Figure 2 shows a non-homogenous surface with Mg-rich bands on the unpolished alloy, as indicate earlier. The difference in corrosion behavior between the polished and unpolished samples proved that the removal of the Mg-rich surface by polishing improved the interaction between the alloy surface and the two types of coatings formed. The results also showed that the corrosion protection promoted by the chromate coating did not prevent corrosion in either surfaces, polished or unpolished. Also, the chromate coating promoted less effective corrosion protection compared with the BTSE for polished samples.

3.3 | Scanning electrochemical microscopy

Figure 10 shows SECM maps for unpolished (A) and polished (B) AA2198-T8 samples. The effect of the NSDL is clearly shown in

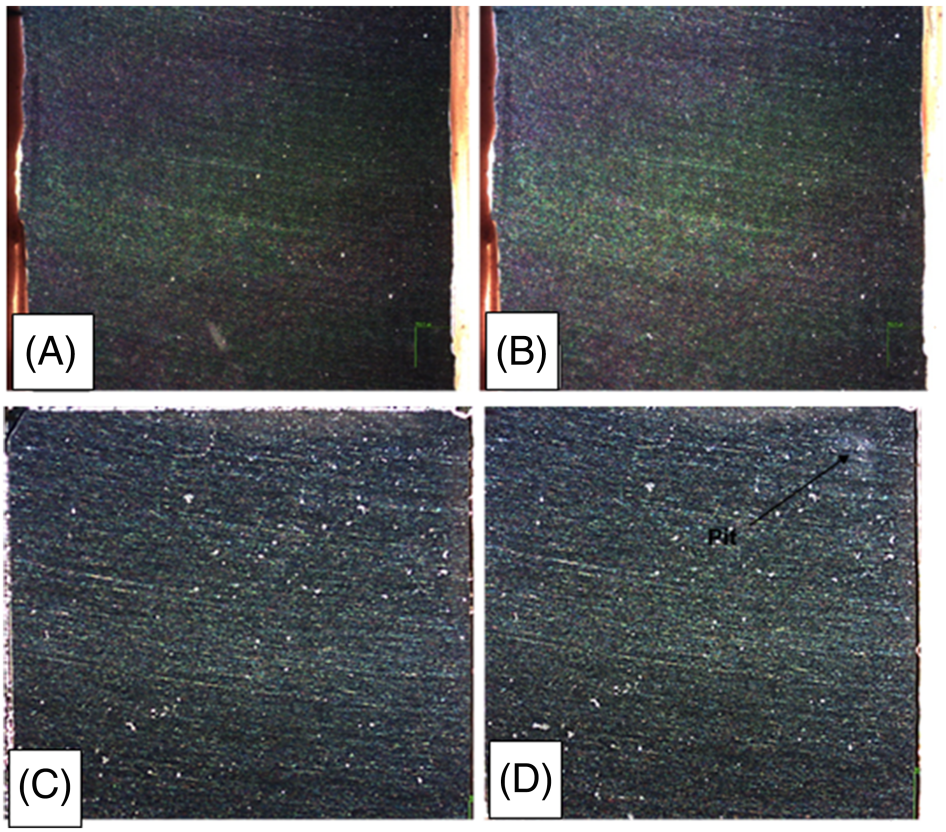

FIGURE 3 Polished AA2198 T8 after exposure to 0.005 mol L^{-1} NaCl solution: coated with BTSE silane film for (A) 2 h and (B) 12 h and with chromate coating after (C) 2 h and (D) 12 h

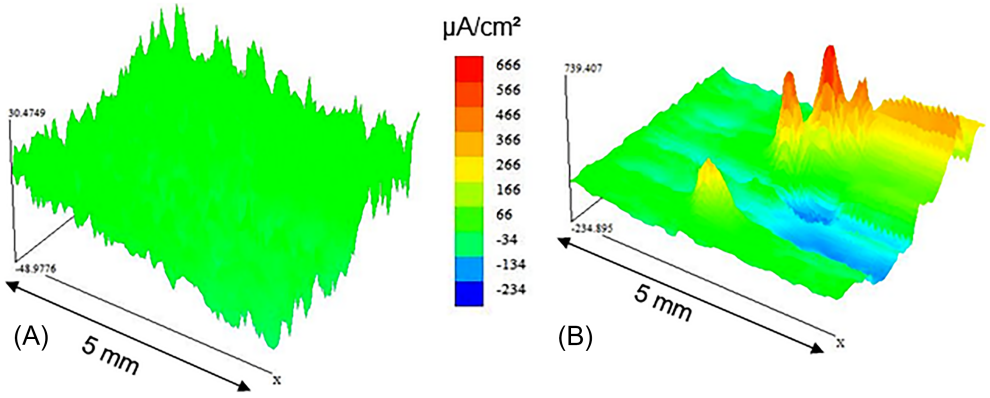

FIGURE 4 SVET maps of unpolished AA2198 T8 coated with BTSE silane film after immersion in 0.005 mol L^{-1} NaCl solution for (A) 2 h and (B) 12 h

the SECM maps. Polished samples were related to more homogeneously distributed currents, Figure 10B, than the unpolished ones, Figure 10A. For the BTSE coated samples, either unpolished, Figure 10C, or polished, Figure 10D, more homogeneous current distribution was obtained than for the bare samples and for the CrVI coated samples, Figure 10E,F. The high currents at some points of the CrVI treated samples are likely due to the high cathode/anode ratio at the weak points of the CrVI coating. The SECM results supported the previous indication by EIS and SVET, showing that the NSDL has a strong influence on the chemical interaction between the BTSE or CrVI coatings and the alloy surface, as suggested earlier.

3.4 | X-ray photoelectron spectroscopy

Figure 11 shows the high-resolution spectra for Al2p region of AA2198 T8 alloy in the polished states for the three different surface treatments described in Section 2. Figure 11A shows the high-resolution spectra for polished AA 2198 T8 nontreated sample. The Al2p was deconvoluted with two components, and the low energy component was assigned to Al° whereas the high energy one was due to Al_2O_3. For polished AA 2198 T8 treated with BTSE, Figure 11B, the Al2p was deconvoluted with three components. There is a well-defined Al° peak at lower energy. The other two components were

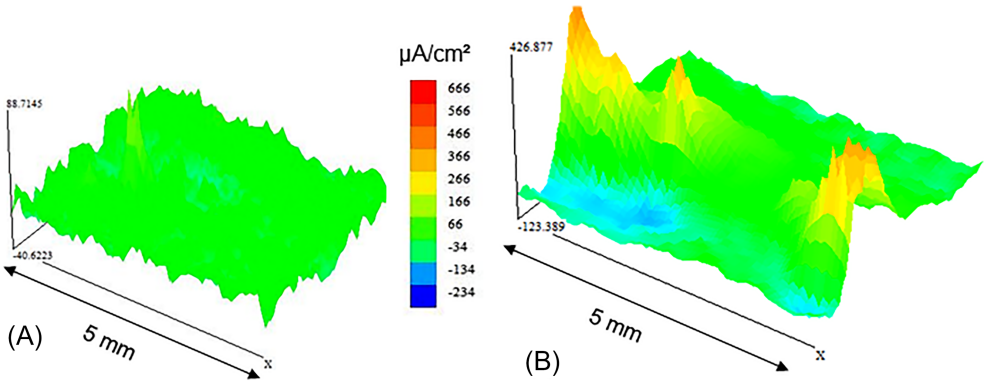

FIGURE 5 SVET maps of unpolished AA2198 T8 treated with CrVI containing solution after immersion in 0.005 mol L^{-1} NaCl solution for (A) 2 h and (B) 12 h

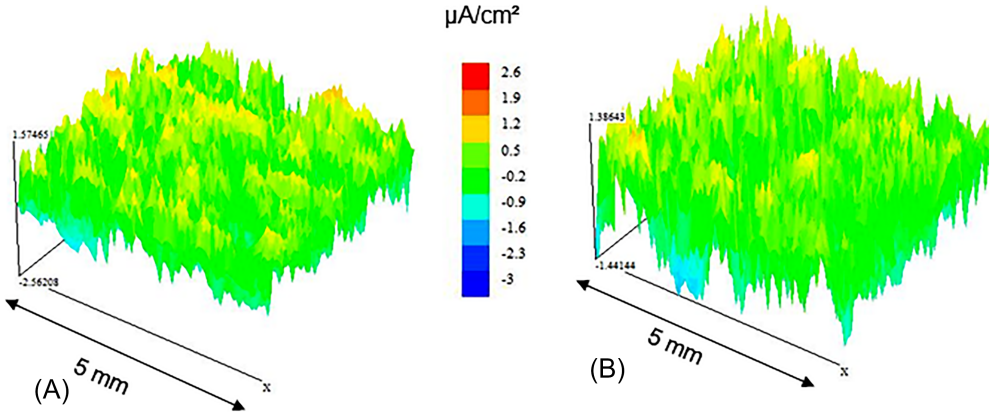

FIGURE 6 SVET maps of polished AA2198 T8 treated with coated with BTSE silane film after immersion in 0.005 mol L^{-1} NaCl solution for (A) 2 h and (B) 12 h

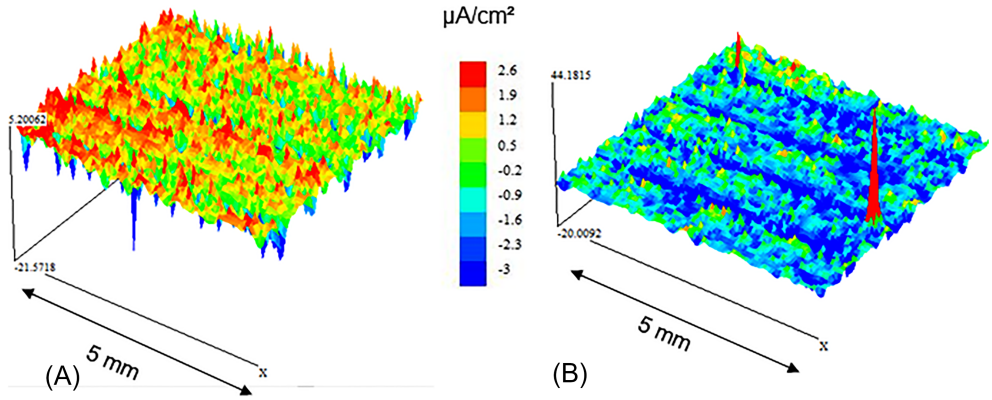

FIGURE 7 SVET maps of polished AA2198 T8 treated with CrVI containing solution after immersion in 0.005 mol L^{-1} NaCl solution for (A) 2 h and (B) 12 h

attributed to Al_2O_3 and Al $(OH)_3$. For the polished AA2198 T8 treated with CrVI, Figure 11C, the Al2p was deconvoluted with three components. The signal of metallic aluminum was clearly detected at the lower energy part of the spectrum. The other two components would be related to Al_2O_3 and Al $(OH)_3$.

Figure 12 shows the high-resolution spectra for Al2p region of AA2198 T8 alloy in the unpolished states for the three different surface treatments described in Section 2. Figure 12A shows the spectra for unpolished AA2198 T8 nontreated, and the Al2p was also detected and deconvoluted with two components. The low energy one is attributed to Al_2O_3 whereas the high energy component is assigned to Al $(OH)_3$.[44–46] Metallic Al peak was not detected. Figure 12B shows the spectra for unpolished AA2198 T8 treated with BTSE. The Al2p was deconvoluted with three components. There is a well-defined metallic Al peak in the lower energy part of the spectrum. The higher energy components were attributed to Al_2O_3 and Al $(OH)_3$. For unpolished AA2198 T8 treated with CrVI, Figure 12C, the spectrum was deconvoluted with two components, Al_2O_3 and Al $(OH)_3$, and no Al° was detected.

Figure 13 shows the high-resolution spectra for O1s region of polished AA2198 T8 nontreated (Figure 13A). The spectra were deconvoluted in two components were attributed to O^{2-} and OH^-, is important to notice that O^{2-} is predominant component with the proportion O_2^-/OH^- in proportions of 4:1. For polished AA 2198 T8

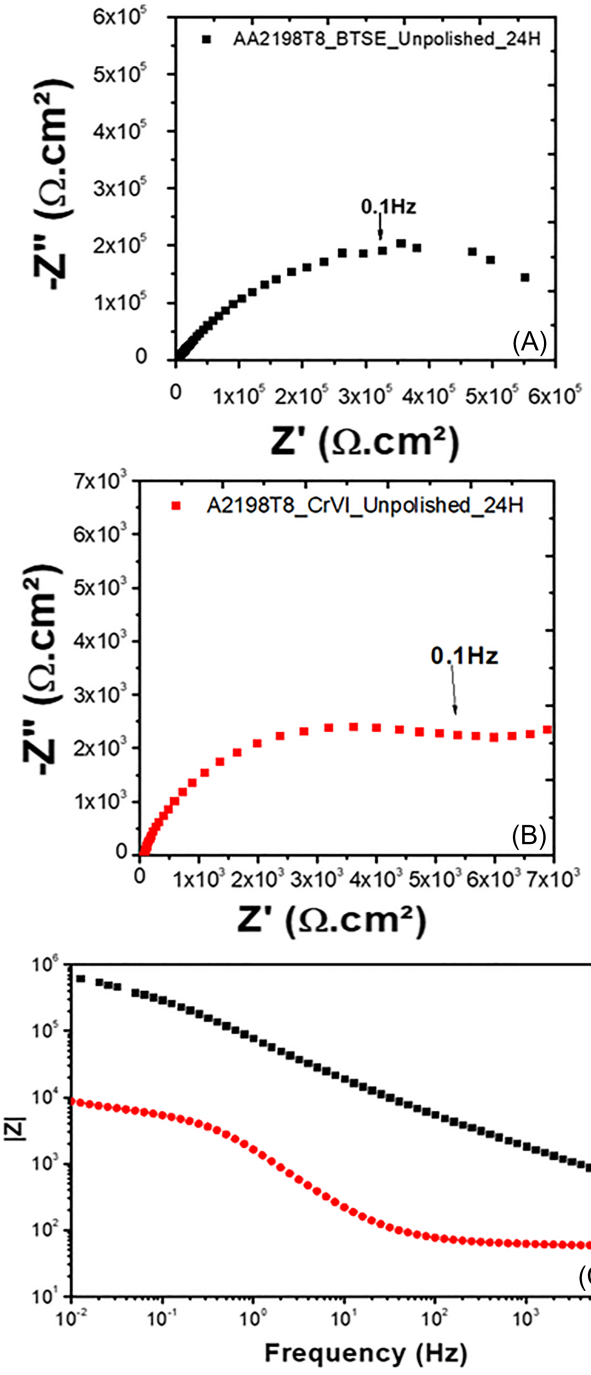

FIGURE 8 Nyquist (A) CrVI, Nyquist (B), and BTSE and comparative BODE diagrams (C) for unpolished AA2198 T8 with surface treatments after 24 h in 0.1 mol L^{-1} NaCl solution

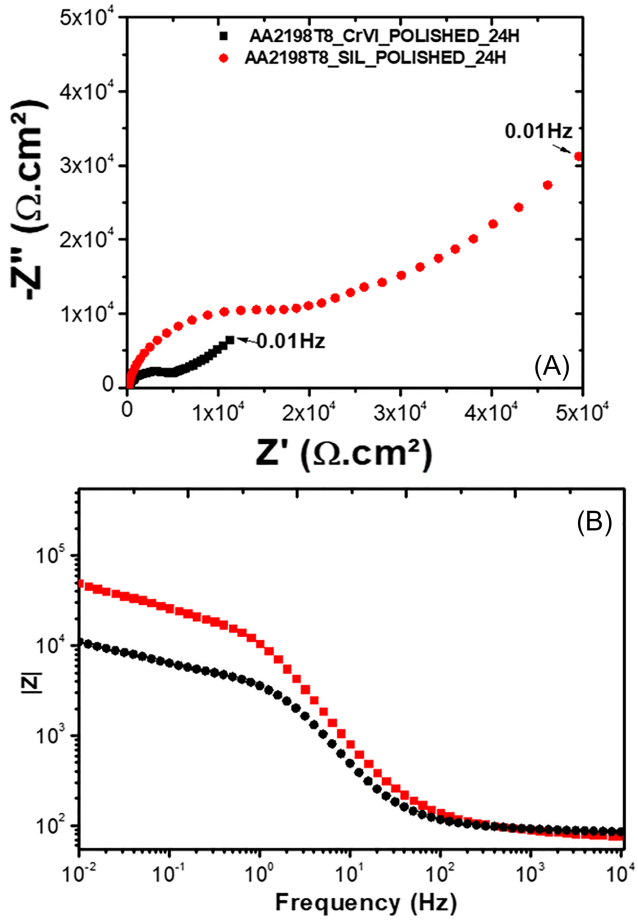

FIGURE 9 Nyquist (A) and Bode diagrams (B) for polished AA2198 T8 with surface treatments after 24 h in 0.1 mol L^{-1} NaCl solution

treated with BTSE (Figure 13B), the O1s was adjusted with only one component assigned to O–Si bonds.[23,35] For polished AA 2198 T8 treated with CrVI (Figure 13C, the O1s was adjusted with only one component assigned to O^{2-} bonds.[47]

Figure 14 shows the high-resolution spectra for O1s region of unpolished AA2198 T8 (Figure 14A. The spectra were also deconvoluted in two components and were attributed to O^{2-} and OH^{-} for both conditions.[44,48] It is important to notice that in the unpolished condition (Figure 14A), the proportion O^{2-}/OH^{-} is well balanced, 1:1 differently from the polished one for which O^{2-} is the predominant component, in proportion of 4:1. It could be related with the detected Mg signal on the unpolished surfaces caused by the presence of NDSL. According to these results, all Mg would be present as $Mg(OH)_2$. In Figure 14B, the O1s spectrum was also deconvoluted in two components which were attributed to O^{2-} and OH^{-}, differently from the polished sample (Figure 13B), that was adjusted with only one component assigned to O–Si bonds.[23,35] For unpolished AA2198-T8 treated with CrVI, Figure 14C, the O1s was adjusted with only one component assigned to O^{2-} bonds.[47]

Figure 15 shows the high-resolution spectra for the polished AA2198-T8 sample, Figure 15A. The Si2p spectrum was fitted with only one component, attributed to Si–O–Si bonds that are typically during the silanization process. It suggests that silanization was successful, as Si–O–C bonds were not observed. For the polished AA2198 T8 treated with BTSE and polished AA2198 T8 nontreated, the spectra of Li1s, Mg1s, and Zr3d have no signal. Figure 15B shows the high-resolution spectra in the Si2p region for the unpolished AA2198 T8 alloy. The Si2p spectrum was fitted with only one

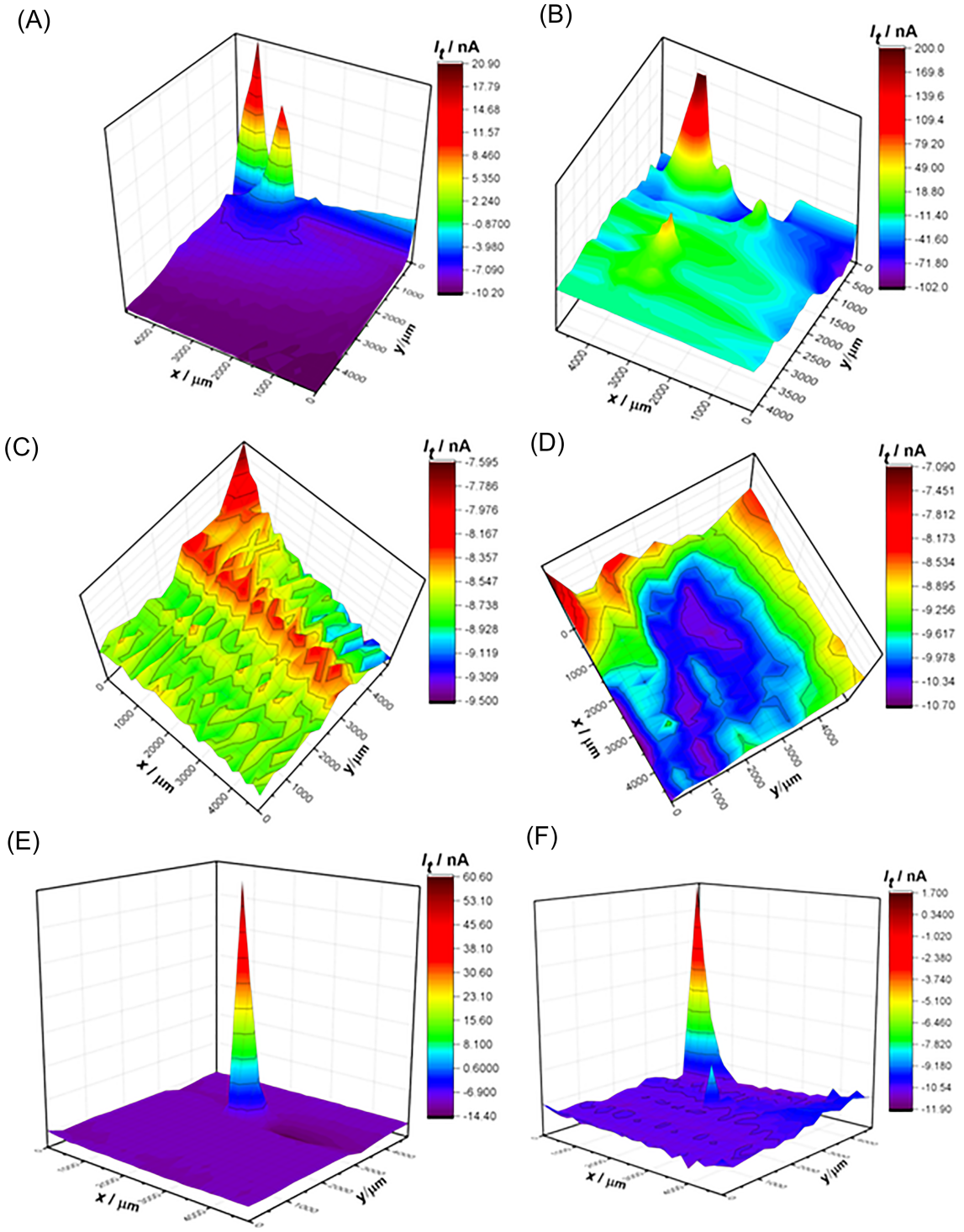

FIGURE 10 SECM maps of polished and unpolished AA2198 T8 after immersion in 0.001 mol L^{-1} NaCl solution for 2 h exposure, where (A) polished AA2198-T8 nontreated, (B) unpolished AA2198-T8 nontreated, (C) polished AA2198-T8 coated with BTSE, (D) unpolished AA2198-T8 coated with BTSE, (E) polished AA2198-T8 treated with CrVI solution, and (F) unpolished AA2198-T8 treated with CrVI solution

component, attributed to Si–O–Si bonds that are typically formed during the silanization process. The same behavior was observed for the polished sample, Figure 15A.[23,35,49] It suggests that silanization was also successful, as Si–O–C bonds were not observed. For the unpolished AA2198 T8 treated with BTSE, the Mg1s spectra (Figure 15C) was deconvoluted with one component attributed Mg $(OH)_2$ that has a much more intense signal in this condition in relation to the polished condition, which is in agreement with the presence of the NSDL for the sample without polishing. Likewise, the signal of the Li1s (Figure 15D) was much more intense in the unpolished surface.

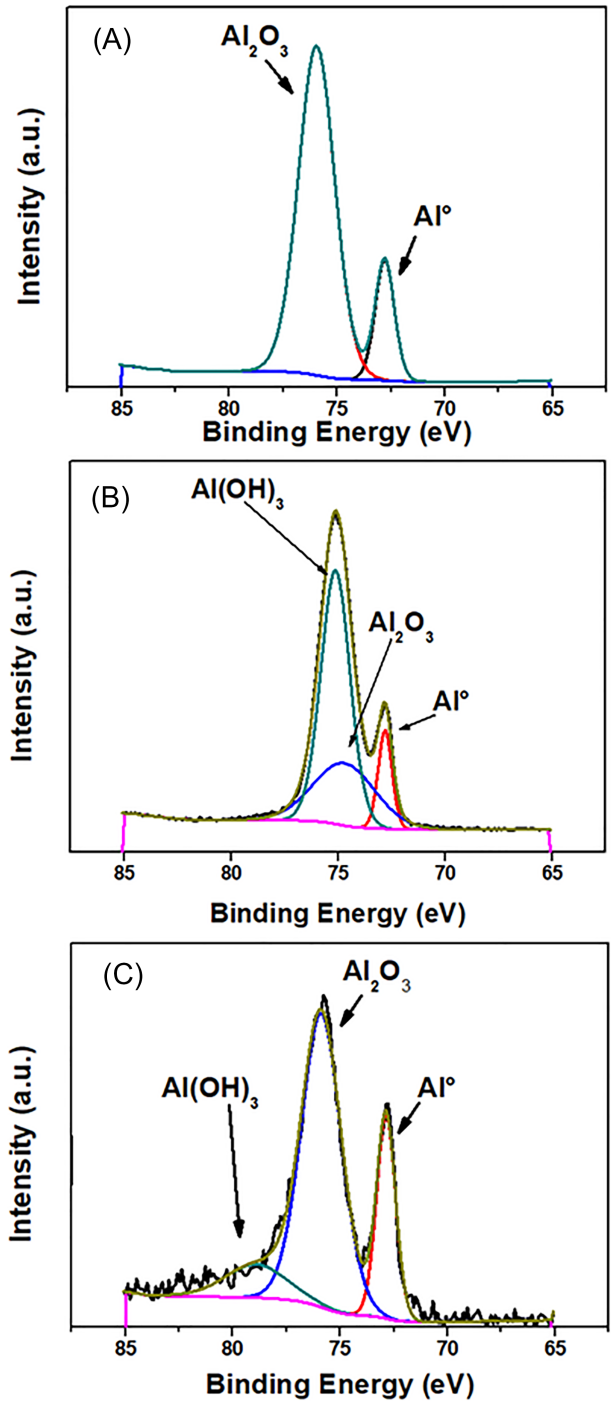

FIGURE 11 XPS high resolution spectra for Al2P region: (A) polished AA2198 T8 nontreated, (B) polished AA2198 T8 treated with BTSE, and (C) polished AA 2198 T8 treated with CrVI

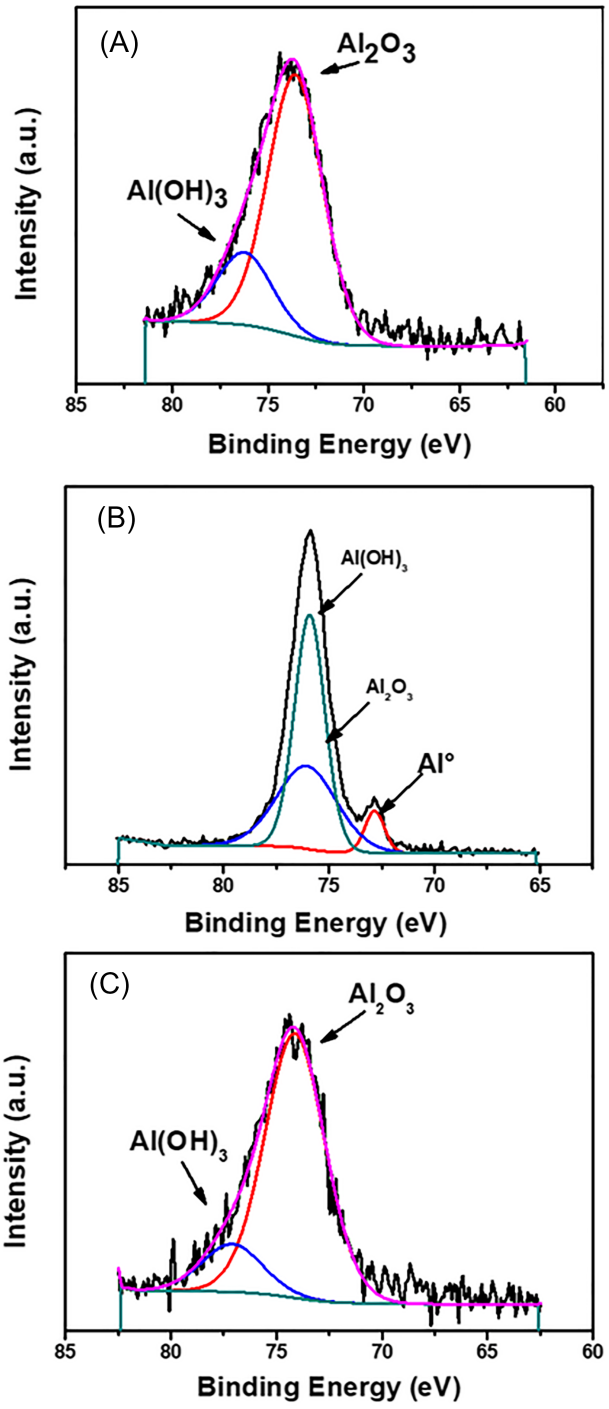

FIGURE 12 XPS high resolution spectra for Al2P region: (A) unpolished AA2198 T8 nontreated, (B) unpolished AA2198 T8 treated with BTSE, and (C) unpolished AA 2198 T8 treated with CrVI

Figure 16A shows the high-resolution spectra for Cr2p region of polished AA2198 T8 treated with CrVI. The Cr2p spectrum was deconvoluted with three components. There is a mixture of oxidation states 3^+ and 6^+ (higher energy) in spectra.[47] It is important to notice the presence of chromium in the 6^+ oxidation state which is the main responsible for corrosion protection of chromium-treated Al alloys.[50,51] For the high-resolution spectra for Cr2p region of unpolished AA2198 T8 treated with CrVI, Figure 16B, the Cr2p spectrum was also deconvoluted with three components, revealing a mixture of oxidation states 3^+ and 6^+ (higher energy).

In the polished state the Li1s signal was detected in the high resolution spectra in the polished one treated with CrVI (Figure 16C),

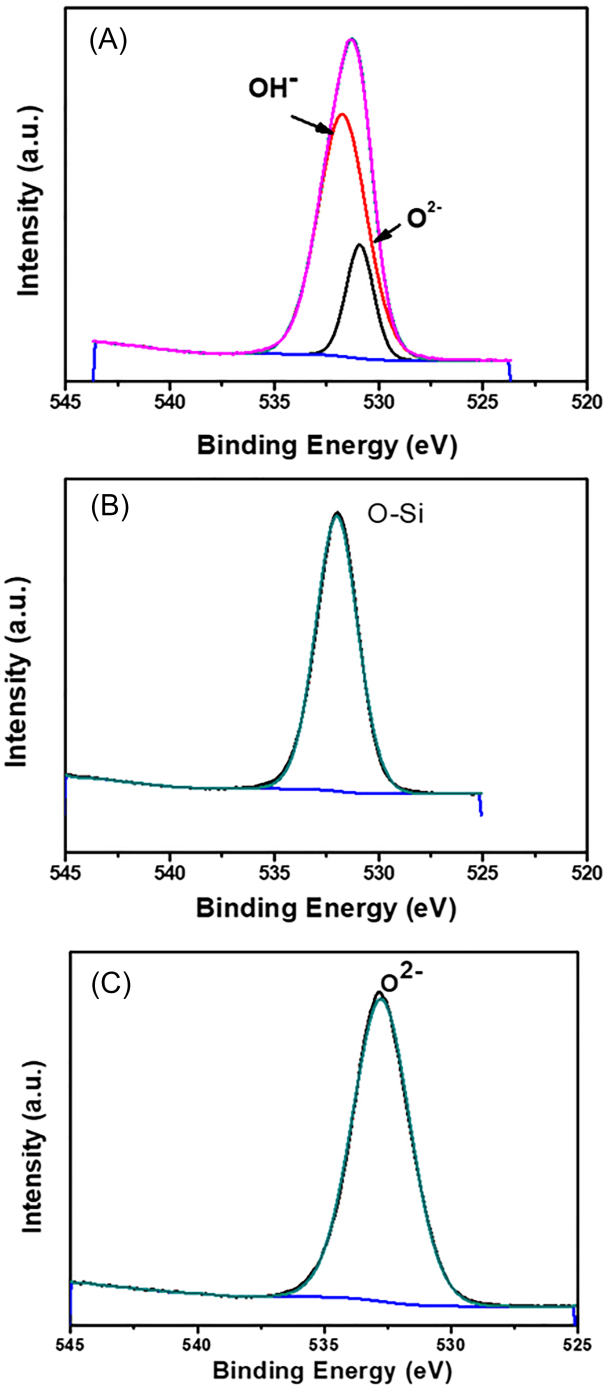

FIGURE 13 XPS high resolution spectra for O1s region: (A) polished AA2198 T8 nontreated, (B) polished AA2198 T8 treated with BTSE, and (C) polished AA 2198 T8 treated with CrVI

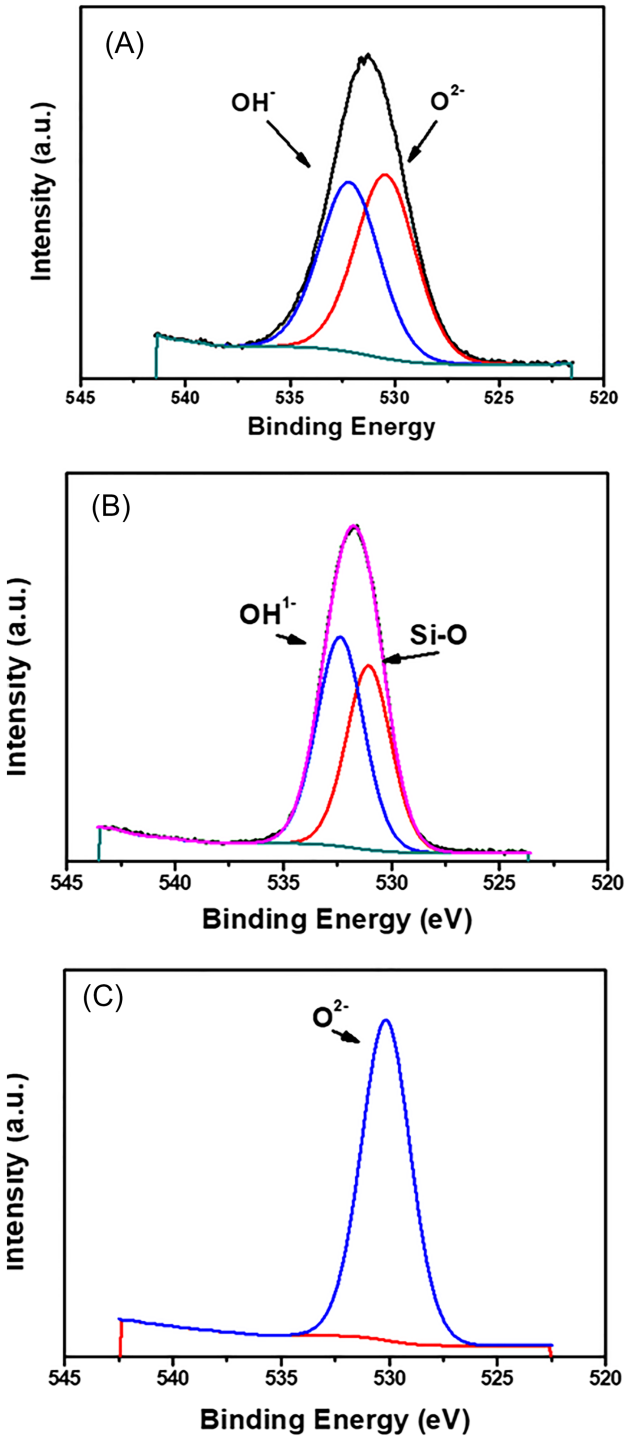

FIGURE 14 XPS high resolution spectra for O1s region: (A) unpolished AA2198 T8 nontreated, (B) unpolished AA2198 T8 treated with BTSE, and (C) unpolished AA 2198 T8 treated with CrVI

where the NSDL is not formed and in the unpolished one (Figure 16D). In the polished AA2198 treated with CrVI, the Mg1s spectra (Figure 16D) showed a weak signal. For the unpolished AA2198 T8 treated with CrVI, the signal of the Mg1s (Figure 16E) is more intense in relation to the polished condition, which would be in accordance with the presence of NSDL.

Figure 17 shows the survey spectra of polished and unpolished AA2198-T8 treated with BTSE (Figure 17A) and treated with CrVI (Figure 17B). It is important to notice that the NSDL affects the degree of deposition of Si, attributed to Si–O–Si component, as showed earlier in Figure 15. This result is in accordance with the lower corrosion protection performance of the unpolished surface

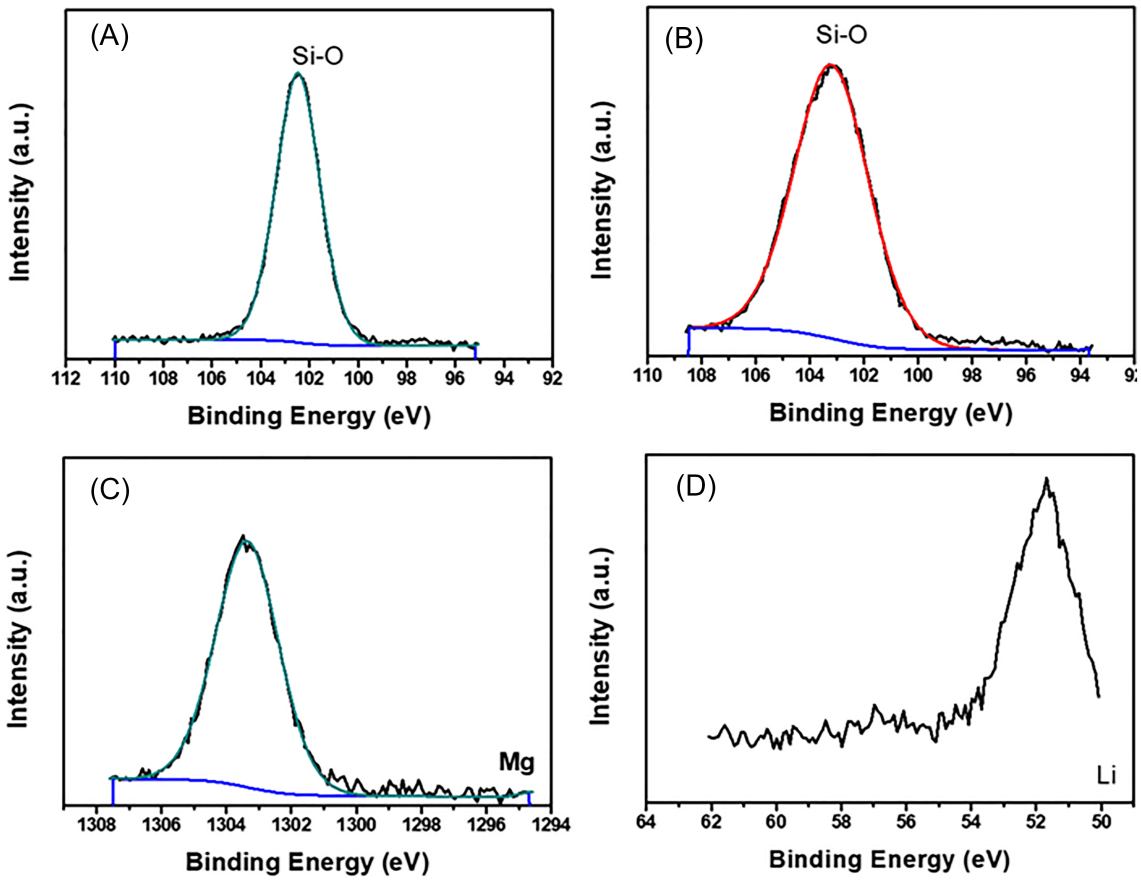

FIGURE 15 XPS high resolution spectra: (A) Si2p for polished AA 2198 T8 coated with BTSE and (B) for unpolished AA2198 T8 coated with BTSE, (C) Mg1s for unpolished AA2198 T8 coated with BTSE, and (D) Li1s for unpolished AA2198 T8 coated with BTSE

when compared with the polished one. Figure 17B shows that the polished AA2198-T8 treated with CrVI presents a more intense signal for Cr than the unpolished sample. As such, slightly lower amounts of CrVI are detected on the unpolished surface which is in accordance with the corrosion performance evaluation. As revealed in the SVET and SECM maps, the polished CrVI treated sample presented higher corrosion protection ability than the unpolished one.

4 | DISCUSSION

It has been shown that NSDL affects the results of corrosion performance in both treatments. It is important to notice that the quality of silane films is improved by the presence of hydroxyl groups on the surface.[24,28,31,33] Hydroxyl groups are important because of the mechanism of siloxane film formation on the metallic surface, Figure 18, is caused by a reaction of silanol groups in the condensed BSTE molecules present in the bath solution that results in dipole-dipole interactions and attraction forces between oxygen and hydrogen atoms at the interface (chemisorption).[24,28,29,31,33] As showed in the high-resolution spectra for O1s of unpolished AA2198-T8 sample (Figure 15A), the NSDL provides a well-balanced proportion of O^{2-}/OH^{-}, and the high resolution spectra of Al2p show a strong peak of Al $(OH)_3$ that connect with the SiOH groups resulting in the AlOSi bonding formed after cross-link, Figure 18.

The polished surface (without NSDL) presented an intense peak for hydroxyl groups, as showed in the high-resolution spectra for O1s of unpolished AA2198-T8, Figure 16A, and a very active metallic surface. It is interesting to notice that the alloy presents hydroxyl groups for both conditions (polished and unpolished). This result is in accordance with the good corrosion performance observed by SVET, SECM, and EIS results, suggesting that a silane film with good quality was obtained due to a successful silanization process which is related to the absence of Si–O–C bonds on the silane-treated surfaces. The relatively poor corrosion performance of the unpolished condition with respect to the polished one was expected, due to the effect of the NSDL on silanization. Many authors have reported that the NSDL affects the corrosion behavior of different Al alloys,[41,52–57] although the influence of this layer on the third (new) generation of Al–Cu–Li alloys has been rarely reported.[23] In the present

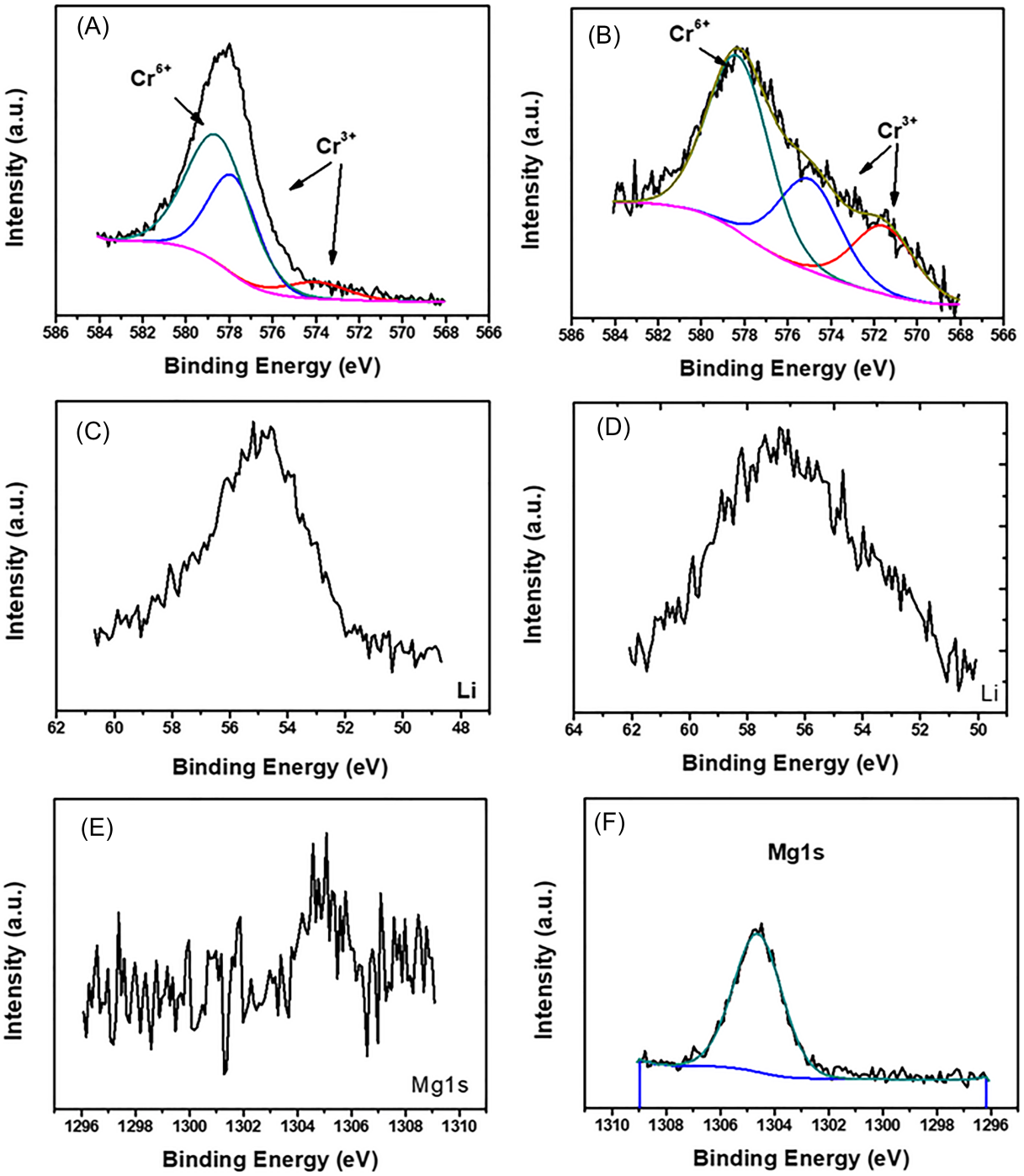

FIGURE 16 XPS high resolution spectra for Cr2p region (A) polished AA2198 T8 treated with CrVI and (B) for unpolished AA2198 T8 treated with CrVI, (C) for Li1s region of polished AA 2198 T8 treated with CrVI, (D) for Li1s region of unpolished AA 2198 T8 treated with CrVI, (E) for Mg1s for polished AA 2198 T8 treated with CrVI, and (F) for Mg1s for unpolished AA 2198 T8 treated with CrVI

study, it is suggested that the poor corrosion protection ability of the unpolished samples coated with BTSE is caused by the heterogeneous surface related to the highly active surface corresponding to Mg-enriched bands regions of the unpolished samples, Figure 3, leading to preferential sites for localized corrosion.[22,23,37,58] The XPS signal for the unpolished sample showed more intense peaks for Mg and Li as expected, and it resulted in a surface electrochemically more active than the polished one, as showed in the SECM maps, Figure 12C,D.

In a bid to understand the interaction of the AA2198-T8 surface with the chromate conversion coating, it is important to notice the conversion layer is formed according to the depicted in Equations 2

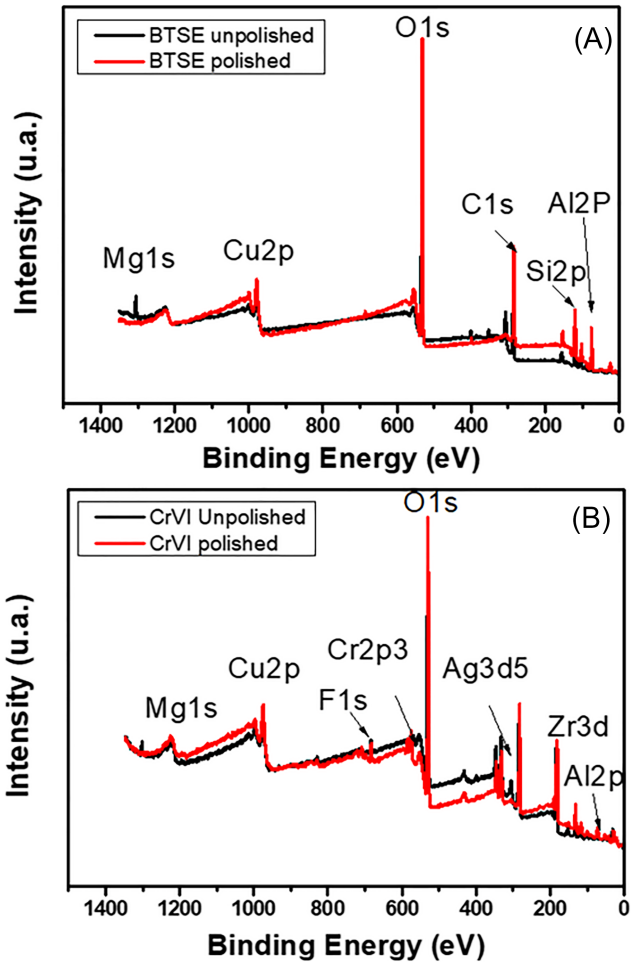

FIGURE 17 XPS survey spectra for (A) unpolished and polished AA2198 T8 coated with BTSE and (B) unpolished and polished treated with CrVI

and 3. CrVI is incorporated in the chromate layer according to the general model proposed by equilibria of CrVI, Equation 4.[50] The formation of conversion layer on aluminum alloys requires free fluoride in the solution to break the thin aluminum oxide on the surface, Equations 5 and 6.[54,59]

$$2Al \rightarrow 2Al^{3+} + 6e^{-}, \tag{2}$$

$$Cr_2O_7^{2-} + 8H^{+} + 6e^{-} \rightarrow 2Cr(OH)_3 + H_2O, \tag{3}$$

$$CrIII(OH) + CrVI_{aq} + H^{+} \leftrightarrow Cr(III) - O - Cr(VI) + H_2O, \tag{4}$$

$$Al_2O_3.3H_2O + 6H^{+} \rightarrow 2Al^{3+} + 6H_2O, \tag{5}$$

$$Al^{3+} + 6F^{-} \rightarrow AlF_6^{3-}. \tag{6}$$

As the surface of the unpolished AA2198-T8 sample presents significant amounts of Li and Mg, as it was shown by the XPS spectra of both conditions, these elements hinder the formation of the chromate layer. As Li and Mg are more active than Al, these elements have a strong influence at the reactions occurring by competing with aluminum, Equations 7 and 8, forming LiF and MgF_2.

$$Li^{+} + F^{-} \rightarrow LiF, \tag{7}$$

$$Mg^{2+} + 2F^{-} \rightarrow MgF_2. \tag{8}$$

Consequently, the corrosive attack of the chromating solution to the aluminum oxide/hydroxide is reduced and, therefore, the Al_2O_3 layer cannot be completely removed freeing the surface for the formation of chromium hydroxide. This affects directly the contact between the active aluminum surface and the chromate bath solution resulting in poor nucleation and growth of the chromate layer over the whole surface,[50,60] thus influencing chromate layer continuity on the surface.

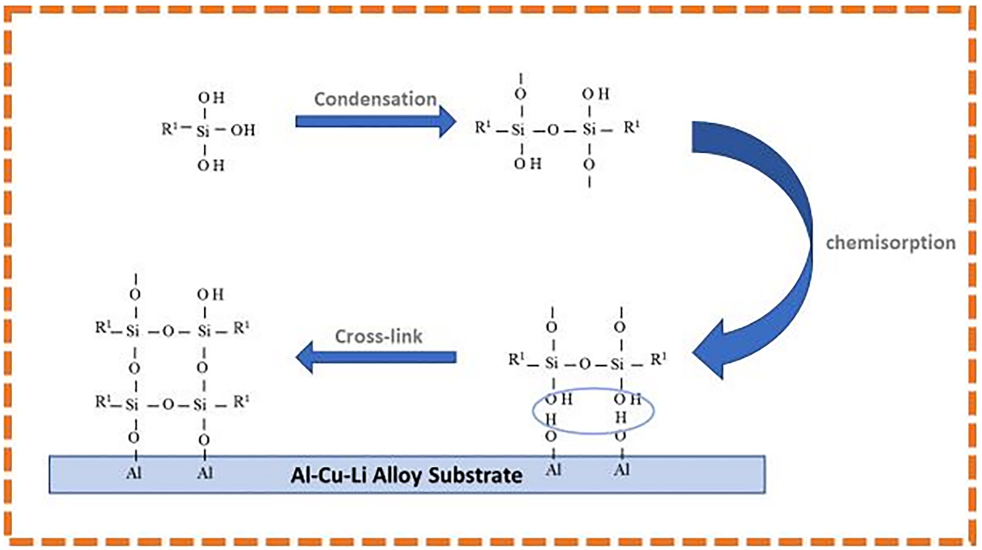

FIGURE 18 Mechanism of silane formation

5 | CONCLUSIONS

The corrosion resistance of the AA2198-T8 with two surface conditions, either unpolished (with NSDL) or polished (without NDSL), prior to treatment for coatings formation, either BTSE or chromate (CrVI), was investigated and compared in this work. The conclusions from the results obtained are as follows:

- The corrosion protection provided by the BTSE coating on the polished surfaces was superior to that of the chromate (CrVI) layer.
- Neither the BTSE coating nor the chromate one was related to effective corrosion protection for the surface with NSDL (unpolished AA2198-T8 samples), due to Mg-rich bands at the surface of the unpolished alloy.
- The NSDL has a significant effect on the alloy corrosion protection ability of the coatings tested in this study, BTSE, and CrVI.
- The BTSE is an effective coating for corrosion protection of Al-Cu-Li alloys and could replace chromate (CrVI) coating with improved corrosion performance and with the advantage of not generating toxic residues.

ACKNOWLEDGEMENT

The authors are grateful to Conselho Nacional de Desenvolvimento Científico e Tecnológico (CNPq) (Proc. 426280/2016-4) for the financial support to this work.

ORCID

Rafael Emil Klumpp https://orcid.org/0000-0003-3851-3277
Uyime Donatus https://orcid.org/0000-0001-8871-3571
Rejane Maria Pereira da Silva https://orcid.org/0000-0003-0081-8323
Renato Altobelli Antunes https://orcid.org/0000-0003-1540-6495
Caruline de Souza Carvalho Machado https://orcid.org/0000-0003-4172-119X
Mariana Xavier Milagre https://orcid.org/0000-0003-2048-2863
João V. de Sousa Araujo https://orcid.org/0000-0001-6375-0480
Bárbara Victoria Gonçalves de Viveiros https://orcid.org/0000-0002-0990-1839
Isolda Costa https://orcid.org/0000-0002-4987-3334

REFERENCES

1. Rioja RJ, Liu J. The evolution of Al-Li base products for aerospace and space applications. *Metall Mater Trans a Phys Metall Mater Sci*. 2012;43(9):3325-3337. https://doi.org/10.1007/s11661-012-1155-z
2. Prasad NE, Gokhale AA, Rao PR. Mechanical behaviour of aluminium-lithium alloys. *Sadhana*. 2003;28(1–2):209-246. https://doi.org/10.1007/BF02717134
3. Buchheit RG, Moran JP, Stoner GE. Electrochemical behavior of the T1 (Al_2CuLi) intermetallic compound and its role in localized corrosion of Al-2% Li-3% Cu alloys. *Corrosion*. 1994;50(2):120-130. https://doi.org/10.5006/1.3293500
4. Li JF, Li CX, Peng ZW, Chen WJ, Zheng ZQ. Corrosion mechanism associated with T1 and T2 precipitates of Al-Cu-Li alloys in NaCl solution. *J Alloys Compd*. 2008;460(1–2):688-693. https://doi.org/10.1016/j.jallcom.2007.06.072
5. Zhang X, Liu B, Zhou X, et al. Corrosion behavior of friction stir welded 2A97 Al-Cu-Li alloy. *Corrosion*. 2017;73(8):988-997, 2418. https://doi.org/10.5006/2418
6. Nayan N, Yadava M, Sarkar R, et al. Microstructure and tensile response of friction stir welded Al–Cu–Li (AA2198-T8) alloy. *Mater Charact*. 2020;159:1-12, 110002. https://doi.org/10.1016/j.matchar.2019.110002
7. Zhang X, Liu B, Zhou X, et al. Laser welding introduced segregation and its influence on the corrosion behaviour of Al-Cu-Li alloy. *Corros Sci*. 2018;135:177-191. https://doi.org/10.1016/j.corsci.2018.02.044
8. Luo C, Albu SP, Zhou X, et al. Continuous and discontinuous localized corrosion of a 2xxx aluminium-copper-lithium alloy in sodium chloride solution. *J Alloys Compd*. 2016;658:61-70. https://doi.org/10.1016/j.jallcom.2015.10.185
9. Donatus U, de Viveiros BVG, de Alencar MC, et al. Correlation between corrosion resistance, anodic hydrogen evolution and microhardness in friction stir weldment of AA2198 alloy. *Mater Charact*. 2018;144:99-112. https://doi.org/10.1016/j.matchar.2018.07.004
10. Huang J, Li JF, Liu DY, et al. Correlation of intergranular corrosion behaviour with microstructure in Al-Cu-Li alloy. *Corros Sci*. 2018;139 (April 2017):215-226. https://doi.org/10.1016/j.corsci.2018.05.011
11. Zhang X, Zhou X, Hashimoto T, et al. Corrosion behaviour of 2A97-T6 Al-Cu-Li alloy: the influence of non-uniform precipitation. *Corros Sci*. 2018;132:1-8. https://doi.org/10.1016/j.corsci.2017.12.010
12. Zhang X, Zhou X, Hashimoto T, et al. The influence of grain structure on the corrosion behaviour of 2A97-T3 Al-Cu-Li alloy. *Corros Sci*. 2017;116:14-21. https://doi.org/10.1016/j.corsci.2016.12.005
13. Victor J, Araujo DS, Donatus U, et al. On the severe localized corrosion susceptibility of the AA2198-T851 alloy. *Corros Sci*. 2018;133 (December 2017):132-140. https://doi.org/10.1016/j.corsci.2018.01.028
14. Buchheit RG, Moran JP, Stoner GE. Localized corrosion behavior of alloy 2090—the role of microstructural heterogeneity. *Corrosion*. 1990;46(8):610-617. https://doi.org/10.5006/1.3585156
15. Wang J, Zhou X, Thompson GE, Hunter JA, Yuan Y. Microstructure evolution in the near-surface region during homogenization of a twin-roll cast AlFeMnSi alloy. *Metall Mater Trans a Phys Metall Mater Sci*. 2016;47(8):4268-4275. https://doi.org/10.1007/s11661-016-3568-6
16. Donatus U, Terada M, Ramirez C, et al. On the AA2198-T851 alloy microstructure and its correlation with localized corrosion behaviour. *Corrosion Science*. 2018;131(December 2017):300-309. https://doi.org/10.1016/j.corsci.2017.12.001
17. Prasad NE, AA Gokhale, RJH Wanhill, eds. Microstructure and precipitate characteristics of aluminum-lithium alloys. *Aluminum-Lithium Alloys Processing, Properties, and Applications* (pp. 99-137, Chapter 4). Butterworth-Heinemann; 2014. ISBN 978-0-12-401698-9. https://doi.org/10.1016/B978-0-12-401698-9.00017-3
18. Ma Y, Zhou X, Liao Y, et al. Localised corrosion in AA 2099-T83 aluminium-lithium alloy: the role of grain orientation. *Corrosion Science*. 2016;107:41-48. https://doi.org/10.1016/j.corsci.2016.02.018
19. Harvey TG. Cerium-based conversion coatings on aluminium alloys: a process review. *Corros Engeening Sci Technol*. 2013;48(4):248-269. https://doi.org/10.1179/1743278213Y.0000000089
20. Kulinich SA, Akhtar AS. On conversion coating treatments to replace chromating for Al alloys: recent developments and possible future directions 1. *Russ J Non-Ferrous Met*. 2012;53(2):176-203. https://doi.org/10.3103/S1067821212020071
21. Klumpp RE, Donatus U, Araujo JVS, Redígolo MM, de SC Machado C, Costa I. The effect of acid pickling on the corrosion behavior of a cerium conversion-coated AA2198-T851 Al-Cu-Li alloy. *J Mater Eng Perform*. 2020;29(1):167-174. https://doi.org/10.1007/s11665-019-04551-9

22. de SC Machado C, Klumpp RE, Ayusso VH, et al. Effect of surface treatments on the localized corrosion resistance of the AA2198-T8 aluminum lithium alloy welded by FSW process. *Surf Interface Anal*. 2019;51(12):1231-1239.
23. Donatus U, Klumpp RE, Vardan Mogili NV, Antunes RA, Milagre MX, Costa I. The effect of surface pretreatment on the corrosion behaviour of silanated AA2198-T851 Al-Cu-Li alloy. *Surf Interface Anal*. 2019;51(2):275-289. https://doi.org/10.1002/sia.6584
24. Franquet A, Terryn H, Vereecken J. Study of the effect of different aluminium surface pretreatments on the deposition of thin non-functional silane coatings. *Surf Interface Anal*. 2004;36(8):681-684. https://doi.org/10.1002/sia.1735
25. Child TF, Van Ooij WJ. Application of silane technology to prevent corrosion of metals and improve paint adhesion. *Trans Inst Met Finish*. 1999;77(2):64-70. https://doi.org/10.1080/00202967.1999.11871249
26. Jiang MY, Wu LK, Hu JM, Zhang JQ. Silane-incorporated epoxy coatings on aluminum alloy (AA2024): part 2: mechanistic investigations. *Corros Sci*. 2015;92:127-135. https://doi.org/10.1016/j.corsci.2014.11.048
27. Xiao W, Man R, Miao C, Peng T. Study on corrosion resistance of the BTESPT silane cooperating with rare earth cerium on the surface of aluminum-tube. *J Rare Earths*. 2010;28(1):117-122. https://doi.org/10.1016/S1002-0721(09)60063-6
28. Zucchi F, Frignani A, Grassi V, Balbo A, Trabanelli G. Organo-silane coatings for AZ31 magnesium alloy corrosion protection. *Mater Chem Phys*. 2008;110(2–3):263-268. https://doi.org/10.1016/j.matchemphys.2008.02.015
29. Demopoulos J. Corrosion resistance of silane coatings on aluminum and magnesium alloys. *Honor Res Proj*. 2017;551:1-25. https://doi.org/10.1002/9780470531778
30. Palanivel V, Zhu D, Van Ooij WJ. Nanoparticle-filled silane films as chromate replacements for aluminum alloys. *Prog Org Coatings*. 2003;47(3–4):384-392. https://doi.org/10.1016/j.porgcoat.2003.08.015
31. Van Ooij WJ, Zhu D, Stacy M, et al. Corrosion protection properties of organofunctional silanes—an overview. *Tsinghua Sci Technol*. 2005;10(6):639-664.
32. Hooshmand S, Peikari M, Zaarei D, Danaei I. Electrochemical effects of silane pretreatments containing cerium nitrate on cathodic disbonding properties of epoxy coated steel. *J Adhes Sci Technol Sci Technol*. 2013;27:2411-2420.
33. Franquet A, Biesemans M, Terryn H, Willem R, Vereecken J. Study of the interaction of hydrolysed silane solutions with pre-treated aluminium substrates. *Surf Interface Anal*. 2006;38:172-175. https://doi.org/10.1002/sia.2251
34. Susac D, Leung CW, Sun X, Wong KC, Mitchell KAR. Comparison of a chromic acid and a BTSE final rinse applied to phosphated 2024-T3 aluminum alloy. *Surf Coatings Technol*. 2004;187(2–3):216-224. https://doi.org/10.1016/j.surfcoat.2004.03.017
35. Brusciotti F, Batan A, De Graeve I, et al. Characterization of thin water-based silane pre-treatments on aluminium with the incorporation of nano-dispersed CeO_2 particles. *Surf Coatings Technol*. 2010;205(2):603-613. https://doi.org/10.1016/j.surfcoat.2010.07.052
36. Palomino LM, Suegama PH, Aoki IV, Fatima Montemor M, De Melo HG. Electrochemical study of modified non-functional bis-silane layers on Al alloy 2024-T3. *Corros Sci*. 2008;50(5):1258-1266. https://doi.org/10.1016/j.corsci.2008.01.018
37. Donatus U, Ferreira RO, Vardan Mogili NV, Gonçalves de Viveiros BV, Milagre MX, Costa I. Corrosion and anodizing behaviour of friction stir weldment of AA2198-T851 Al-Cu-Li alloy. *Mater Chem Phys*. 2018;219(August):493-511. https://doi.org/10.1016/j.matchemphys.2018.08.053
38. Liu Y, Hashimoto T, Zhou X, et al. Influence of near-surface deformed layers on filiform corrosion of AA3104 aluminium alloy. *Surf Interface Anal*. 2013;45(10):1553-1557. https://doi.org/10.1002/sia.5232
39. Liu Y, Zhou X, Thompson GE, Hashimoto T, Scamans GM, Afseth A. Precipitation and corrosion behaviour of nano-structured near-surface layers on an AA6111 aluminium alloy. *J Phys Conf Ser*. 2006;26(August):103-106. https://doi.org/10.1088/1742-6596/26/1/024
40. Liu Y, Laurino A, Hashimoto T, et al. Corrosion behaviour of mechanically polished AA7075-T6 aluminium alloy. *Surf Interface Anal*. 2010;42(4):185-188. https://doi.org/10.1002/sia.3136
41. Scamans GM, Frolish MF, Rainforth WM, et al. The ubiquitous Beilby layer on aluminium surfaces. *Surf Interface Anal*. 2010;42(4):175-179. https://doi.org/10.1002/sia.3204
42. Donatus U, Klumpp RE, Mogili NVV, Altobelli Antunes R, Milagre MX, Costa I. The effect of surface pretreatment on the corrosion behaviour of silanated AA2198-T851 Al-Cu-Li alloy. *Surf Interface Anal*. 2019;51(2):275-289. https://doi.org/10.1002/sia.6584
43. Donatus U, Terada M, Ospina CR, Queiroz FM, Bugarin AF, Costa I. On the AA2198-T851 alloy microstructure and its correlation with localized corrosion behaviour. *Corros Sci*. 2018;131:300-309. https://doi.org/10.1016/j.corsci.2017.12.001
44. Shimizu K, Phanopoulos C, Loenders R, Abel M, Watts JF. The characterization of the interfacial interaction between polymeric methylene diphenyl diisocyanate and aluminum: a ToF-SIMS and XPS study †. *Surf Interface Anal*. 2010;42(December 2009):1432-1444. https://doi.org/10.1002/sia.3586
45. Hinder SJ, Grilli R, Rustame M, Santos WIA, Baker MA, Costa I. A surface analytical investigation of cerium-based conversion coatings deposited onto an AA2024-T3 aluminium alloy cladding layer. *Surf Interface Anal*. 2014;46(February):735-739. https://doi.org/10.1002/sia.5440
46. Heller DK, Fahrenholtz WG, O'Keefe MJ. The effect of post-treatment time and temperature on cerium-based conversion coatings on Al 2024-T3. *Corros Sci*. 2010;52(2):360-368. https://doi.org/10.1016/j.corsci.2009.09.023
47. Biesinger MC, Brown C, Mycroft JR, Davidson RD, Mcintyre NS. X-ray photoelectron spectroscopy studies of chromium compounds. *Surface and interface analysis: an international journal devoted to the development and application of techniques for the analysis of surfaces, interfaces and thin films*. 2004;36(12):1550-1563. https://doi.org/10.1002/sia.1983
48. Kibel MH. X-ray photoelectron spectroscopy. In: O'Connor J, Sexton B, Smart R, eds. *Surface Analysis Methods in Materials Science*. Springer-Verlag Berlin; 2003:175-201 doi:10.1007/978-3-662-05227-3_7.
49. Palomino LM, Suegama PH, Aoki IV, Montemor MF, De Melo HG. Electrochemical study of modified cerium—silane bi-layer on Al alloy 2024-T3. *Corros Sci*. 2009;51(6):1238-1250. https://doi.org/10.1016/j.corsci.2009.03.012
50. Schram T, de Wit JHW, Campestrini P, Terryn H, Böhm S. Study of the formation of chromate conversion coatings on Alclad 2024 aluminum alloy using spectroscopic ellipsometry. *Thin Solid Films*. 2002;410(1–2):76-85. https://doi.org/10.1016/S0040-6090(02)00253-5
51. Gharbi O, Thomas S, Smith C, Birbilis N. Chromate replacement: what does the future hold? *npj Mater Degrad*. 2018;2:23-25. https://doi.org/10.1038/s41529-018-0034-5
52. Afseth A, Nordlien JH, Scamans GM, Nisancioglu K. Effect of heat treatment on electrochemical behaviour of aluminium alloy AA3005. *Corros Sci*. 2002;44:145-162.
53. Afseth A, Nordlien J, Scamans G, Nisancioglu K. Effect of heat treatment on filiform corrosion of aluminium alloy AA3005. *Corros Sci*. 2001;43:2093-2109.
54. Wang S-S, Yang F, Frankel GS. Effect of altered surface layer on localized corrosion of aluminum alloy 2024. *J Electrochem Soc*. 2017;164(6):C317-C323. https://doi.org/10.1149/2.1541706jes
55. Frankel G. The effects of microstructure and composition on Al alloy corrosion. *Corrosion*. 2015;71(11):1308-1320.

56. Donatus U, Thompson GE, Zhou X, Alias J, Tsai IL. Grain distinct stratified nanolayers in aluminium alloys. *Mater Chem Phys*. 2017;188:109-114. https://doi.org/10.1016/j.matchemphys.2016.12.021
57. Donatus U, de Viveiros BVG, de Alencar MC, Ferreira RO, Milagre MX, Costa I. Correlation between corrosion resistance, anodic hydrogen evolution and microhardness in friction stir weldment of AA2198 alloy. *Mater Charact*. 2018;144:99-112. https://doi.org/10.1016/j.matchar.2018.07.004
58. de SC Machado C, Donatus U, Milagre MX, et al. Correlating the modes of corrosion with microstructure in friction stir welded AA2198-T8 alloy in aqueous hydrogen peroxide-chloride medium. *Corrosion*. 2019;75(6):628-640. https://doi.org/10.5006/3054
59. Hugues AE, Taylor RJ, Nelson KJW, Hinton BRW, Wilson L. Characterisation of surface preparation of 2024 aluminium alloy for conversion coating. *Mater Sci Technol*. 1996;12(11):928-936. https://doi.org/10.1179/mst.1996.12.11.928
60. Campestrini P, Van Westing EP, De Wit JH. Influence of surface preparation on performance of chromate conversion coatings on Alclad 2024 aluminium alloy part I: nucleation and growth. *Electrochim Acta*. 2001;46:2553-2571.

How to cite this article: Klumpp RE, Donatus U, da Silva RMP, et al. Corrosion protection of the AA2198-T8 alloy by environmentally friendly organic-inorganic sol-gel coating based on bis-1,2-(triethoxysilyl) ethane. *Surf Interface Anal*. 2021;53:314–329. https://doi.org/10.1002/sia.6919